Available online at www.sciencedirect.com
SCIENCE DIRECT®
Journal of Solid State Chemistry 178 (2005) 1526–1532
JOURNAL OF SOLID STATE CHEMISTRY
www.elsevier.com/locate/jssc

Advances in the structure and microstructure determination of yttrium silicates using the Rietveld method

Carla Cannas[a], Anna Musinu[a], Giorgio Piccaluga[a], Claudio Deidda[b], Filomena Serra[b], Marco Bazzoni[b], Stefano Enzo[b,*]

[a]*Dipartimento di Scienze Chimiche, Cittadella Universitaria di Monserrato, S.S. 554 Bivio per Sestu, 09042 Cagliari, Italy*
[b]*Dipartimento di Chimica, via Vienna n. 2, 07100 Sassari, Italy*

Received 14 October 2004; received in revised form 23 February 2005; accepted 25 February 2005
Available online 24 March 2005

Abstract

The Y_2O_3–SiO_2 1:1 composition doped with a weak concentration of europium ions was prepared with the sol–gel technique and the products studied by X-ray diffraction as a function of temperature in the range from 900 to 1300 °C, using the method of Rietveld for quantitative evaluation of amorphous and crystalline evolving phases. The amorphous profile of the yttrium oxyorthosilicate glasses has been described following the "Rietveld for Disordered Materials" method and subsequently included in the patterns of semicrystalline samples that have been heat-treated for temperatures above 900 °C at 1000, 1100, 1150, 1200 and 1300 °C. The quantitative evaluation of the amorphous phase is obtainable from the Rietveld approach equivalent to the method after Ruland. This enabled us to study in fine detail the structural rearrangements and growth mechanisms that take place during the crystal-to-amorphous transformation in terms of coordination numbers, average interatomic distances, average crystallite size and microstrain and to identify the polymorphous transformation involving the Y_2SiO_5 phase from low-to-high-temperature forms, as well as some minor quantities of other phases namely α-$Y_2Si_2O_7$ phase, Y_2O_3 and $Y_{4.67}(SiO_4)_3O$.

Keywords: Sol–gel synthesis; Semicrystalline systems; Amorphous-to-crystal transformation; Kinetics; Powder X-ray diffraction; Crystallinity; Rietveld refinement

1. Introduction

The Y_2O_3–SiO_2 phase diagram [1] is currently being explored with a variety of synthesis techniques and below 1400 °C especially in the 1:1 and 1:2 molar ratio because of the optical properties that can be induced by dispersion in the matrix of rare-earth elements such as Eu^{3+}, Tb^{3+} and Ce^{3+}. In correspondence to the 1:1 molar ratio, the compound Y_2SiO_5 is polymorphous according to two monoclinic forms X_1 and X_2 of space group $P2_1/c$ n. 14 and $B2/b$ n. 15, respectively [2,3]. The structural transformation between the X_1 and X_2 forms occurs near to 1200 °C [4] and, in general, the host lattice of the X_2 form is thought to be more suitable than the X_1 form for luminescence applications due to the difficulty in obtaining pure single phase X_1-Y_2SiO_5 and possibly to the different coordination of yttrium atoms, which eventually are supposed to be substituted for by the rare-earth element. The second compound in the system is Y_2O_3–$2SiO_2$, which show an even more complex polymorphism, since six $Y_2Si_2O_7$ different structures are reported for it, namely α, β, γ, δ, *y* and *z*. Mixed powder routes and sol–gel processes have been used for the synthesis of these materials and the range of phase stability is being investigated as a function of heat treatment. Crystallization of amorphous sol–gel yttrium oxyorthosilicate samples is qualitatively observed around 900 °C [5] and subsequent high-temperature phase transformations are determined mainly from

*Corresponding author. Fax: +39 079 229559.
E-mail address: enzo@uniss.it (S. Enzo).

0022-4596/$ - see front matter © 2005 Elsevier Inc. All rights reserved.
doi:10.1016/j.jssc.2005.02.024

powder X-ray diffraction (XRD) patterns. However, the structural investigations hitherto reported were substantially qualitative and no comparisons of the new structural data with existing investigations were discussed in numerical terms apart from one exception dealing with the low temperature phases of R_2SiO_5 (R = rare-earth elements) [4].

In this paper we have synthesized by sol–gel technique the Y_2O_3–SiO_2 composition doped with a weak concentration of europium ions, and we report the quantitative structural analysis by the Rietveld method, which has made possible to follow the evolution from the amorphous matrix up to crystallization at 1300 °C.

2. Synthesis approach

Yttrium nitrate ($Y(NO_3)_3 \cdot 6H_2O$, Aldrich, 99%), europium nitrate [$Eu(NO_3)_3 \cdot 3.5H_2O$], Tetraethoxysilane (TEOS, Aldrich, 98%) and absolute ethanol (Carlo Erba 99.8%) were used as reactants in the sol–gel preparation. Aqueous solutions containing appropriate concentrations of yttrium and europium nitrates to give a Eu/Y ratio of 0.001 were mixed with an ethanolic solution of TEOS and acidified with nitric acid. The resulting sol was stirred for 180 min at room temperature and then allowed to gel at 50 °C. The gelation time was of about 3 days. The white dry gels, X-ray amorphous, were fragmented and powdered in an agate mortar and subjected to calcination at the temperature of 900, 1000, 1100, 1150, 1200 and 1300 °C for 2 h. The concentration of europium ions in the final samples was checked through a plasma ICP Perkin-Elmer 2000 and it turned out to be the nominal ($Eu_{0.002}Y_{1.998}O_3$–SiO_2).

3. X-ray diffraction and the evaluation of crystallinity fraction

The samples were investigated with a Seifert diffractometer ID 3000 using Cu$K\alpha$ wavelength, with a graphite monochromator in the diffracted beam. Because of the high-resolution mode needed for the specimens, which are treated at high temperature, the XRD patterns were collected with narrow divergent and antiscatter slits (0.5°), a receiving slit width of 0.1 mm and a step size of 0.04° in the 2θ angular range from 12° to 80°. The crystalline phases were retrieved after a peak search semi-automatic routine using the data base PDF-2 [6].

In the case of semicrystalline materials, Ruland [7] developed an XRD method for evaluating the amount of crystalline phases in an otherwise amorphous matrix. After defining the variable $s = 2\sin\theta/\lambda$, integrating the volume of substance over the whole of reciprocal space and normalizing, the crystallinity x_{cr} was expressed as

$$x_{cr} = \frac{\int_{s_0}^{s_p} I_c(s)s^2\,ds}{\int_{s_0}^{s_p} I(s)s^2\,ds} \frac{\int_{s_0}^{s_p} \bar{f}^2(s)s^2\,ds}{\int_{s_0}^{s_p} \bar{f}^2(s)D(s)s^2\,ds}, \quad (1)$$

where $I(s)$ is the total diffracted intensity, $I_c(s)$ the intensity due only to crystalline phases, $D(s)$ is a "disorder" function, $\bar{f}^2(s)$ the squared average scattering factor (coherent + incoherent) calculated with respect to the chemical composition of the sample and s_o and s_p the lower and upper limits of integration, respectively. The equation is normally split into two factors:

$$R(s_p) = \frac{\int_{s_0}^{s_p} I(s)s^2\,ds}{\int_{s_0}^{s_p} I_c(s)s^2\,ds} \text{ and } K(s_p) = \frac{\int_{s_0}^{s_p} \bar{f}^2(s)s^2\,ds}{\int_{s_0}^{s_p} \bar{f}^2(s)D(s)s^2\,ds}. \quad (2)$$

In the absence of disorder (a condition always holding at the origin of the reciprocal space) $D(s) = 1$, so that Ruland used to extrapolate to $s = 0$ the ascending behaviour observed in a $R(s_p)$ vs. s_p^2 plot due to the background, incoherent scattering contributions and to disorder effects. Originally, the separation of the amorphous profile from the crystalline Bragg peaks was accomplished by tracing empirically a continuous line. Later, further extensions were proposed in order to computerize the procedure [8] and to account for the case where the crystalline component separates from the amorphous matrix with a different atomic density [9].

Using the Rietveld analysis, Riello et al. [10,11] proposed a solution of the problem of semicrystalline materials due to the presence of an amorphous phase when its chemical composition or the global sample composition was known. From then, essentially two different lines of work have been proposed within the Rietveld context: the first uses an internal standard and determines the amorphous fraction by difference between the measured and expected value of the standard fraction [12,13], while the second attempts to model the amorphous scattering in a theoretically sound fashion "compatible" with the structural rules of the Rietveld method. Though both approaches have their own merits, the limitations of the first can be easily recognized since it is assumed that the scattering contribution of the amorphous component is a part of the background.

For this reason we have developed further the second line of work, suggested originally by Lutterotti et al. [14], which in turn is based on previous work by Le Bail [15]. Accordingly, the Rietveld approach may in principle account for the structure of amorphous samples, once the user is able to supply a reasonable "pseudo-crystalline" structure factor. In the case of

amorphous silica, Le Bail started from the $P2_12_12_1$ crystalline structure factor of SiO_2 in a Rietveld refinement and reported the modified structure and microstructure parameters which gave a satisfactory agreement between calculated data and XRD and/or neutron diffraction experiments. The limits of such procedure were discussed in comparison with the Reverse Monte Carlo technique [16]. After calibrating the procedure in samples with known quantity of amorphous SiO_2 and crystalline Al_2O_3, Lutterotti et al. [14], found that such an approach, can supply the quantitative analysis of the phases including the amorphous component avoiding the use of any internal standard. This performance of the Rietveld method seems trustworthy in as much as the atomic density is not too different from that of the crystalline counterpart [17] and a similar behaviour must hold for the nearest neighbour interatomic distances.

The structures of the phases (whether crystalline or amorphous) were then inserted in the final refinement using the MAUD program [18] according to the basic equation of the Rietveld method:

$$y_{ci} = S\sum_k L_k \left|\sum_k N_j f_j \exp\left[2\pi i(hx_j + ky_j + lz_j)\right] \times \exp\left(-B_j \sin^2\frac{\theta}{\lambda^2}\right)\right|^2 \varphi(2\theta_i - 2\theta_k)P_k A + y_{bi}, \quad (3)$$

where symbols have the same meaning as in [19].

Capabilities and limitations of the Rietveld refinement from powder diffraction data have been largely expounded [19]. Basically, under the general assumption of a normal distribution of residuals (i.e., the difference between calculated and experimental data points), the program is able to supply, within a fair degree of confidence that in turn depends on the signal-to-noise ratio of the pattern, the quantitative analysis of the phases in the sample, their structural parameters such as unit cell dimensions, crystallographic position of atoms, as well as the microstructure parameters like the average crystallite size, anisotropy and the average lattice microstrain. Because in our patterns we have collected the intensities in a preset-time mode and $\sigma = 1/\sqrt{N}$, we expect that a correct fit give uniform distribution of the difference between the *square root* of calculated and experimental intensities rather than the simple linear difference of the two.

4. Results and discussion

4.1. Amorphous, semicrystalline and crystalline oxyorthosilicate samples

Fig. 1 shows the XRD patterns (logarithmic scale) of Y_2O_3–SiO_2 gels annealed 2 h at the quoted temperatures.

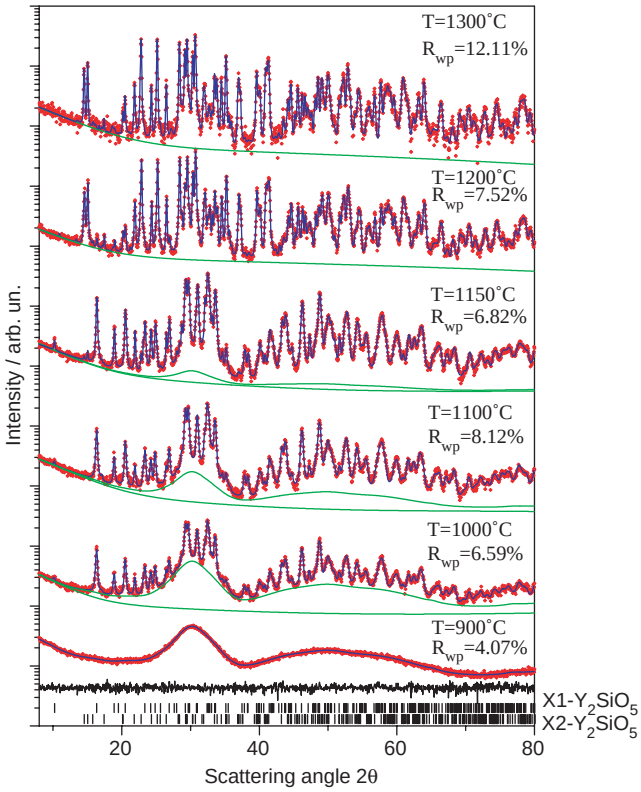

Fig. 1. XRD patterns (data points) and Rietveld refinement (full lines) of yttrium oxyorthosilicate samples as a function of heat treatment at the indicated temperatures. Bar sequences of the peak positions expected from the geometry and lattice parameters of the considered phases (fingerprints) are reported at the bottom. Moreover, the residual curve refers to the difference between square root of calculated and experimental intensities of the sample heat treated at 1000 °C. The agreement factor R_{wp} of fits are also shown.

As usual, data points are from experiment and full lines are intensities calculated after the fit. At 900 °C the sample is still "X-ray" amorphous with a typical first halo at $2\theta = 29.8°$, followed by a second broad band with relative maximum at 2θ around 48°. We may note that the main halo position of the present system is located midway between a minimum value of $2\theta = 22°$ observed for the case of pure amorphous silica and the largest values of 2θ around 40° pertaining to the glassy metals. Even in this case we have used the same arguments of Le Bail [15] and Lutterotti et al. [14] to fit the amorphous profile of the XRD pattern starting from the known X_1-Y_2SiO_5 structure factor of the low-temperature crystalline phase (space group $P2_1/c$ n. 14). The results are reported numerically in Table 1 as it concerns the relevant structure parameters. The values quoted can at best only be one of an ensemble of configurations that would fit the data equally well. In order to pursue further the reliability of the model, data at higher values of the s scattering vector should be collected as it was done by Le Bail [15] for the case of silica glass, which is equivalent to searching for a more

Table 1
Lattice parameters and atom fractional coordinates of the low-temperature structure X_1-Y_2SiO_5 phase used to account for the amorphous profile according to Le Bail (sample heat treated at 900 °C)

Unit cell dimensions $a = 8.50(\pm0.09)$ Å, $b = 6.82(\pm0.04)$ Å, $c = 6.38(\pm0.05)$ Å, $\beta = 104(\pm1)^\circ$

Atom	x	y	z
Y1	0.11(±0.01)	0.13(±0.02)	0.31(±0.03)
Y2	0.46(±0.01)	0.62(±0.04)	0.24(±0.02)
Si1	0.15(±0.04)	0.66(±0.08)	0.32(±0.06)
O1	0.26(±0.04)	0.36(±0.07)	0.61(±0.08)
O2	0.77(±0.06)	0.11(±0.08)	0.15(±0.08)
O3	0.23(±0.05)	0.52(±0.08)	0.002(±0.004)
O4	0.05(±0.04)	0.44(±0.07)	0.37(±0.07)
O5	0.41(±0.03)	0.37(±0.07)	−0.02(±0.03)

The values quoted are one of an ensemble of configurations able to satisfactorily fit the data.

precise mutual arrangement of atoms from the high-angle $h\,k\,l$ terms.

The X-ray pattern of sample annealed at 1000 °C (second curve from the bottom) represents a challenging target for our methodology since it contains, besides the amorphous phase, two crystalline components also, easily identified with the X_1-Y_2SiO_5 phase and an apatite-like phase $Y_{4.67}(SiO_4)_3O$ [PDF card n. 30-1457, space group $P6_3/m$ n. 176], whose refined values are $a_0 = 9.368(2)$ Å and $c_0 = 6.735(2)$ Å, respectively, see also [20]. As it is customary in the Rietveld fit, at the bottom of the patterns we have reported bar sequences of the peak positions (fingerprints) expected from the geometry and lattice parameters of the considered phases. The background line (also plotted) varies slowly and is always positive, which gives further support to the proposed solution in terms of phase constitution. The amorphous profile component, whose parameters have been fixed to the values retrieved in the pure amorphous Y_2O_3–SiO_2 sample annealed at 900 °C, is plotted above the background line and turns out to be 40.0 (±2.0) wt%. The apatite-like phase $Y_{4.67}(SiO_4)_3O$ is 9.0 wt% (±1.0) and the X_1-Y_2SiO_5 phase is found to be present at the 51.0 (±3.0) wt% and its lattice parameters are in fair agreement with those reported by Ito and Johnson in the PDF card n. 41-0004 (also quoted incompletely by Liu et al. [21]) and by Wang et al. [4].

Fractional atomic coordinates are also obtained for the two yttrium cations Y_I^{3+} and Y_{II}^{3+} in ninefold and hepta-coordination, respectively, similar to those reported by Wang et al. [4]. In addition, a recent investigation by MAS-NMR of the ^{89}Y sites in the X_1-Y_2SiO_5 phase [22] has shown two well distinct resonance lines for the two coordination sites, the low field one at 75.2 ppm having strong tails with super-lorentzian character. Furthermore, the unit cell volume from our lattice parameters turns out to be 400.0 (±0.5) Å^3, not too distant from the value of 399.0 Å^3 calculated by Liu et al. [23] from Ito and Johnson data in PDF card no. 41-0004.

One obvious question for the present Rietveld technique extended to semicrystalline systems concerns the error bar related to the quantitative determination. A major point involves the atomic density of the "amorphous pseudo-cell" that, in the case of the sample annealed at 900 °C, is 9% smaller than the value of the low-temperature yttrium oxyorthosilicate X_1-Y_2SiO_5. Having transferred the same structure factor for the amorphous phase to higher temperature means that this component is not subjected to chemical density changes during the annealing. As it concerns the crystalline phases, the most critical parameters that may bias the refinement to a considerable extent are those related to the microstructure, e.g., the crystallite size distribution and the lattice strain. It has been noted [24,25] that assuming a Voigtian profile shape for description of peak broadening implies a log-normal-type distribution for the crystallite size skewed at high size values.

The appearance of the apatite-like phase with chemical composition $O/Y = 2.78$, significantly different from that assumed for the matrix ($O/Y = 2.50$) may arise objections related to the precision of the quantitative procedure adopted here. However, the nominal composition of these phases is in principle subjected to changes because of several kinetics, thermodynamics and chemical factors such as meta-stabilisation of off-stoichiometric compounds, impurities in the precursors, different dissolution and/or evaporation rates during thermal treatment, etc. To sum up, our experience suggests that, once all the phases are correctly included, the intrinsic error bar associated with the present quantitative determination can hardly be larger than 3.0%, while the detection limit, though dependent on the structure and microstructure of the specific phase in relation to the others present in the sample, is around 0.5–1%. This detection limit has to be enhanced to a figure of 4–5 wt% in the case of amorphous phases in semicrystalline systems, but can be also lower in the case of simple systems with few crystalline phases, using unconventional X-ray sources.

Confirmation of such detection limits is retrieved from the analysis of the sample heat treated at 1100 °C, whose pattern is reported in Fig. 1, third curve from the bottom, together with background and amorphous component fitting lines extracted from the refinement. The amorphous phase component turns out to be 14.0 wt%. Its existence can hardly be perceived in a linear intensity scale, but it appears well justified in a logarithmic scale of intensity, where the signal-to-background ratio is properly evaluated. As it concerns the lattice parameters of the X_1-Y_2SiO_5 phase structure, which amounts to ca. 77.0 (±3) wt% of the entire

specimen, they remain essentially unchanged with respect to the sample treated at 1000 °C, with a cell volume of 399.8 (±0.5) Å^3. The average crystallite size $\langle d \rangle$ is now 60 (±10) nm and the average lattice strain $\langle \varepsilon \rangle = 0.0020$ (±0.0002). Furthermore, the apatite-like phase $Y_{4.67}(SiO_4)_3O$ now amounts to 13.0 (±1) wt% and its refined lattice parameters are $a_0 = 9.361(\pm 0.001)$ Å and $c_0 = 6.729(\pm 0.0007)$ Å.

The pattern of the specimen heat-treated at 1150 °C (fourth pattern from the bottom) suggests that the amorphous component almost totally disappears. In fact, the quantitative determination gives a 3% value for it, that is, below the estimated detection limits for an amorphous phase. The refinement using crystalline phases retrieved from the PDF-2 data base gives only a slightly superior agreement factor between calculation and experiment to the point that the amorphous component in this specimen is not clearly supported numerically. The X_1-Y_2SiO_5 phase has increased to 83.0 (±2) wt%, with a unit cell volume of 398.3 (±0.5) Å^3, closer to the value reported by Wang et al. [4] from their refinement. The average crystallite size $\langle d \rangle$ remains at 58 (±6) nm, but the lattice strain $\langle \varepsilon \rangle$ decreases slightly to a figure of 0.0015 (±0.0002).

The apatite-like phase $Y_{4.67}(SiO_4)_3O$ now amounts to 12.0 (±1) wt% and its lattice parameters are $a_0 = 9.360(\pm 0.001)$ Å, $c_0 = 6.729(\pm 0.0007)$ Å, not much different from the previous temperature treatment of 1100 °C. In addition to this, we observe here a 2.0 wt% of the high-temperature phase X_2-Y_2SiO_5 with relative lattice parameters $a = 10.400(\pm 0.001)$ Å, $b = 6.719(\pm 0.0007)$ Å, $c = 12.490(\pm 0.001)$ Å and $\beta = 102.54°(\pm 0.05°)$, giving a cell volume of 852.0 (±0.8) Å^3. Wang et al. [4] reported the transition temperature from X_1 to X_2 phase at 1190 °C, while the appearance of the X_2 phase was detected as a function of calcining temperature between 1200 and 1300 °C by Liu et al. [21]. Similarly, Kang et al. [5] observed the crystal structure change of Y_2SiO_5:Ce phosphors after annealing above 1200 °C. It is clear that these temperatures are referring to the almost complete phase transformation and do not disagree with our observation.

In the pattern of the sample annealed at 1200 °C (last but one curve from the top of Fig. 1) there is no amorphous phase and it can be easily seen that X_2-Y_2SiO_5, with its 82.0 (±2) wt% fraction, is the dominant phase. The refined lattice parameters $a = 10.417(\pm 0.001)$ Å, $b = 6.723(\pm 0.0007)$ Å, $c = 12.483(\pm 0.001)$ Å and $\beta = 102.76°(\pm 0.05°)$, give a cell volume of 852.64 (±0.8) Å^3 in excellent agreement with the data of Maksimov et al. [3]. The average crystallite size $\langle d \rangle$ is 110 (±15) nm and the lattice disorder $\langle \varepsilon \rangle = 0.0002$ (±0.0001), certainly small.

Likewise, the X_1 phase and also the high-temperature X_2 phase show two Y^{3+} sites with Y–O six-fold coordination number. The apatite-like phase $Y_{4.67}(SiO_4)_3O$ is present in proportion of 8.0 (±1) wt% with lattice parameters $a_0 = 9.355(\pm 0.001)$ Å and $c_0 = 6.726(\pm 0.0007)$ Å. There is still 3.0 (±1) wt% of the X_1-Y_2SiO_5 form, structural data of which is not possible to be speculated. In addition, there are small quantities of two further phases, namely cubic Y_2O_3 in the concentration of 2.5 wt% (±1) (Space group *Ia*-3, lattice parameter $a_0 = 10.593 \pm 0.001$ Å) and the α-$Y_2Si_2O_7$ phase (triclinic, space group *P*-1, refined lattice parameters $a = 6.596(\pm 0.0007)$ Å, $b = 6.640(\pm 0.0007)$ Å, $c = 12.036(\pm 0.001)$ Å, $\alpha = 94.71° \pm 0.07$, $\beta = 91.14° \pm 0.07$ and $\gamma = 91.79 \pm 0.07$) in the concentration of 3.5 (±1) wt%. The presence of cubic yttria in X_1-Y_2SiO_5:$Eu_{0.01}$ powders prepared by the sol–gel method and heat treated at 1100 °C during 3 h was surmised by Yin et al. [26] from low-temperature emission spectra, though in a structural context different from ours. The presence of the α-$Y_2Si_2O_7$ phase, with lattice parameters slightly different from those reported in the PDF card no. 38-0223, may be related to separation of the small fraction of yttria from the Y_2SiO_5 matrix during the phase transformation according to the simple reaction $2Y_2SiO_5 \rightarrow Y_2O_3 + Y_2Si_2O_7$. Note that, when this occurs, the $Y_2O_3/Y_2Si_2O_7$ weight ratio amounts to ca. 0.65 not far from the outcome of our Rietveld refinement.

Finally, in the pattern of the specimen treated at 1300 °C (top curve of Fig. 1) we do not find any trace of the low-temperature X_1-Y_2SiO_5 phase. The sample consists of 81.0 (±2) wt% of the X_2-Y_2SiO_5 phase (with crystallite size $\langle d \rangle$ grown to 160 ± 20 nm), the rest being due to 7.0 (±1) wt% apatite-like $Y_{4.67}(SiO_4)_3O$ with lattice parameters $a_0 = 9.360(\pm 0.001)$ Å and $c_0 = 6.731(\pm 0.0007)$ Å, 7.0 (±1) wt%, α-$Y_2Si_2O_7$ phase (refined lattice parameters $a = 6.589 \pm 0.0007$ Å, $b = 6.629 \pm 0.0007$ Å, $c = 12.044 \pm 0.001$ Å, $\alpha = 94.66° \pm 0.05$, $\beta = 90.80° \pm 0.05$ and $\gamma = 92.03 \pm 0.05$) and the remaining 5.0% (±1) cubic Y_2O_3 ($a = 10.601 \pm 0.001$ Å).

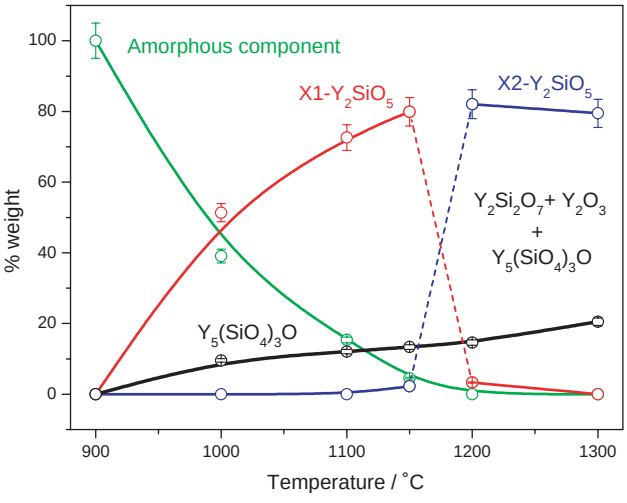

Fig. 2. Kinetics of phase evolution as a function of heat-treatment temperature from quantitative evaluation with the Rietveld method.

Fig. 2 shows the kinetics evolution of the observed phase transformations. Above 900 °C the amorphous phase starts to devitrify, with an exponential decay as a function of the temperature, which is completed at 1150 °C. The full curve of the amorphous component does not interpolate precisely the data evaluated by XRD, probably because we have assumed that the devitrification process starts at 900 °C, so further experiments are necessary to establish precisely this temperature onset. Simultaneously, the low-temperature X_1-Y_2SiO_5 starts to form and reaches its maximum at 1150 °C, while a secondary apatite-like phase $Y_{4.67}(SiO_4)_3O$ gradually increases. Between 1150 and 1200 °C we observe the transformation from low to high-temperature form of Y_2SiO_5. Other minor phases than $Y_{4.67}(SiO_4)_3O$ develop during this process, namely triclinic α-$Y_2Si_2O_7$ and cubic Y_2O_3, which, altogether with the apatite-like phase, seem to be favoured at high temperature at expenses of the X_2-Y_2SiO_5 phase. Of course, more experiments should be done using the present refinement procedure in order to deepen these aspects.

4.2. Comparison with the Ruland method

We have plotted in Fig. 3 the $R(s_p)$ data vs. s^2 of semicrystalline samples heat treated at 1000 and 1100 °C, respectively, after correcting total intensities $I(s)$ for the background (shown in Fig. 1) as determined by the Rietveld approach. Both functions $R(s_p)$ have a similar behaviour in that they initially oscillate and then stabilize in a wide s^2 range corresponding to a 2θ-scale from 40° to 80°, approximately. The important initial oscillations are expected because the integrals appearing in the $R(s_p)$ fraction are computed in a narrow range and are arbitrarily supposed to replace the theoretical

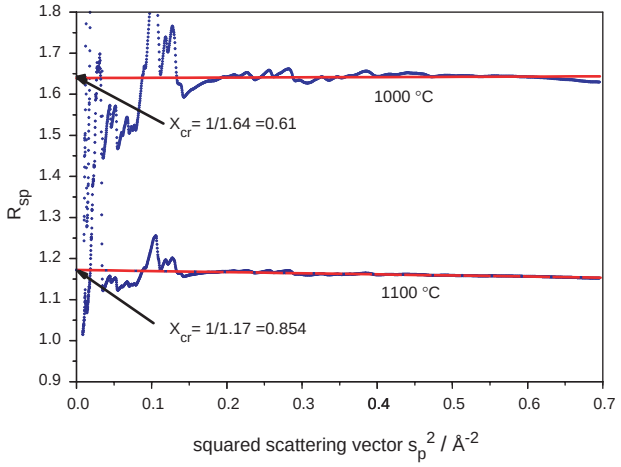

Fig. 3. $R(s_p)$ function of samples treated at 1000 and 1100 °C. According to Ruland, the crystallinity is retrieved from extrapolation to $s^2 = 0$ of the "regular" portion of $R(s_p)$ at wide angles as shown in the inset.

infinite range of integration. Increasing the upper limit of integration makes this approximation (Vainshtein law) better and better respected as it can be assessed by the observed constancy of the $R(s_p)$ factor at higher s, apart from some little oscillations. If we take the inverse of the constant values extrapolated to $s = 0$, as reported in Fig. 3 for the two samples, we obtain crystallinity fractions x_{cr} in very good agreement with the data coming from the Rietveld method, keeping in mind that $x_{am} = (1 - x_{cr})$. For the sample annealed at 1150 °C we expect the $R(s_p)$ curve to oscillate close to 1 (100% crystallinity).

The possibility of verifying texture and accounting for it in terms of different models is peculiar of the Rietveld method, while the Ruland method assumes absence of important anisotropic effects or texture, which, however, is a general pre-requisite in order to fulfil the correctness of the normalization procedure to the total coherent and incoherent independent scattering. The normalisation is carried out in the Rietveld approach when using the scattering factor for each element in the unit cell (or pseudo-unit cell) to calculate and match the observed intensities coming from crystalline and amorphous phases in conjunction with the background separation without considering the incoherent contribution. Also, Ruland [7] and Vonk and Fagherazzi [9] were used to correct the ascending behaviour of $R(s_p)$ function, ascribed to incoherent scattering, disorder of first and second kind type and background, through the $K(s_p)$ function. However, disorder of the first kind is described in the Rietveld approach by the so-called temperature factors Bj of atomic species and we have discussed above the numerical correlations that exist with the background behaviour. On the other hand, disorder of the second kind, also referred to as paracrystalline disorder according to Hosemann and Bagchi [27], refers to lattice strain and is described by the Rietveld codes with various procedures devised to account for the peak overlapping and to separate microstrain from the crystallite size effects. The close agreement with the two methods is also obtained because there is no significant change in composition between crystalline and amorphous component. When this happens in the Ruland method one should apply the corrections reported by Vonk and Fagherazzi [9,28].

5. Conclusions

From the precise analysis of XRD patterns of yttrium oxyorthosilicates according to the Rietveld method a considerable amount of very useful structural and microstructural information can be obtained. The phase analysis was carried out quantitatively, with sufficient degree of precision even in the case of complex peak

envelopes due to the presence of several phases, amorphous and crystalline, as it was verified from the agreement factors of the refinement and from inspection of final residuals, presented just in one case in this work. The refinement technique allows the precise determination of atomic positions in the unit cell which, when coupled with the lattice parameters, supply the interatomic coordination distances. The structural evolution of yttrium oxyorthosilicate material as a function of heat treatment has permitted to follow the amorphous-to-crystalline transformation occurring in the temperature range from 900 to 1100 °C and the most important structural rearrangements pertaining to the low-temperature X_1-Y_2SiO_5 phase. Further analysis of the powder patterns during the refinement allowed to retrieve the presence of other minor phases such as the α-$Y_2Si_2O_7$ phase, Y_2O_3 and $Y_{4.67}(SiO_4)_3O$, showing that the decomposition phenomena may not lead to a polymorphous product. The X_1-Y_2SiO_5 phase is involved in a further transformation to the high-temperature X_2-Y_2SiO_5 form between 1150 and 1200 °C. Average crystallite size and microstrain can be followed for the detected phases across the whole thermal treatment from 900 to 1300 °C.

Acknowledgments

This work is carried out within a collaborative PRIN Project entitled "Nanostructured Luminescent Oxides" funded by the Italian Ministry for Education, University and Science.

Thanks are due to prof. G. Cocco, L. Schiffini, G. Mulas and F. Delogu (Department of Chemistry, University of Sassari, Italy) for many useful discussions on solid state kinetics. We thank Dr. Luca Lutterotti (http://www.ing.unitn.it/~luttero/) for making available a copy of the MAUD program running in a personal computer.

References

[1] E.M. Levin, C.R. Robbins, H.F. McMurdie, Phase Diagram for Ceramists, Fig. 2388, in: M.K. Reser (Ed.), American Ceramic Society, Columbus, OH (USA), 1969.
[2] C. Michel, G. Buisson, E.F. Bertaut, C.R. Acad. Sci. B 264 (1967) 397–399.
[3] B.A. Maksimov, Y.u.A. Kharitonov, V.V. Ilyukhin, N.V. Belov, Dokl. Akad. Nauk SSSR 183 (1968) 1072–1075.
[4] J. Wang, S. Tian, G. Li, F. Liao, X. Jing, Mater. Res. Bull. 36 (2001) 1855.
[5] Y.C. Kang, I.W. Lenggoro, S.B. Park, K. Okuyama, J. Solid State Chem. 146 (1999) 168.
[6] http://www.icsdweb.FIZ-Karlsruhe.de.
[7] W. Ruland, Acta Cryst. (1961).
[8] C.G. Vonk, J. Appl. Cryst. 6 (1973) 148.
[9] C.G. Vonk, G. Fagherazzi, J. Appl. Cryst. 16 (1983) 274.
[10] P. Riello, G. Fagherazzi, P. Canton, D. Clemente, M. Signoretto, J. Appl. Cryst. 28 (1995) 121.
[11] P. Riello, P. Canton, G. Fagherazzi, J. Appl. Cryst. 31 (1998) 78–82.
[12] R.S. Winburn, D.G. Grier, G.J. McCarthy, R.B. Petersen, Powder Diff. 15 (2000) 163.
[13] A.G. De La Torre, S. Bruque, M.A.G. Aranda, J. Appl. Cryst. 34 (2001) 196.
[14] L. Lutterotti, R. Ceccato, R. Dal Maschio, E. Pagani, Mater. Sci. Forum 278–281 (1998) 93.
[15] A. Le Bail, J. Non-Cryst. Solids 183 (1995) 39–42.
[16] R.L. McGreevy, L. Pustzai, Molec. Simul. 1 (1988) 359.
[17] R. Hosemann, A.M. Hindeleh, R. Bruckner, Phys. Status Solidi (a) 126 (1991) 313.
[18] L. Lutterotti, S. Gialanella, Acta Mater. 46 (1998) 101.
[19] R.A. Young (Ed.), The Rietveld Method, University Press, Oxford (UK), 1993.
[20] J. Felsche, J. Solid State Chem. 5 (1972) 266.
[21] Y. Liu, C.N. Xu, K. Nonaka, H. Tateyama, J. Mater. Sci. 36 (2001) 4361.
[22] A.I. Becerro, A. Escudero, P. Florian, D. Massiot, M.D. Alba, J. Solid State Chem. 177 (2004) 2783.
[23] Y. Liu, C.N. Xu, H. Chen, H. Nonaka, Opt. Mater. 25 (2004) 243.
[24] S. Ciccariello, Acta Cryst. A 46 (1990) 175.
[25] S. Enzo, Mater. Sci. Forum 269–272 (1998) 363.
[26] M. Yin, C. Duan, W. Zhang, L. Lou, S. Xia, J.-C. Krupa, J. Appl. Phys. 86 (1999) 3751.
[27] R. Hosemann, S.N. Bagchi, Direct Analysis of Diffraction by Matter, North-Holland, Amsterdam, 1962.
[28] A. Benedetti, M. Bottarelli, G. Fagherazzi, J. Non-Cryst. Solids 74 (1985) 245.